Int. J. of Geosynth. and Ground Eng. (2016) 2:1
DOI 10.1007/s40891-015-0041-3

ORIGINAL ARTICLE

Assessing the Influence of Some Soil–Reinforcement Interaction Parameters on the Performance of a Low Fill on Compressible Subgrade. Part I: Fill Performance and Relevance of Interaction Parameters

Ennio M. Palmeira[1] · **Ivonne A. G. Góngora**[1]

Received: 17 October 2015 / Accepted: 16 December 2015 / Published online: 24 December 2015
© Springer International Publishing Switzerland 2015

Abstract Soil–geosynthetic interaction is a complex subject, particularly in geogrid reinforced structures. Geosynthetic reinforcement can be used to improve the performance of granular layers on compressible subgrades in situations such as paved and unpaved roads and in reinforced foundations. This paper presents results of large scale cyclic loading tests on reinforced and unreinforced granular layers on a compressible subgrade. A woven geotextile and different geogrids were used as reinforcement. The geogrids were chosen aiming at achieving a wide range of values of some physical and mechanical properties to allow the investigation of the influence of some relevant properties related to soil–reinforcement interaction on the geogrid performance. The results obtained showed that geogrid reinforcement tensile stiffness and some of its physical properties such as aperture–fill particle diameter ratio, thickness and fraction of grid area available for bearing are important properties for grid performance as reinforcement in granular layers. A dimensionless parameter taking into account several geogrid properties has been introduced and shows good correlation with test results. On the other hand, no correlation was noted between geogrid aperture stability modulus and granular layer performance for the conditions of the tests carried out. The results show that a geogrid reinforcement should not be specified based only on its tensile stiffness and strength, since other properties play important roles in the gravel layer performance. This is particularly relevant for reinforced unpaved roads and railway tracks.

Keywords Geosynthetics · Reinforcement · Soil–geogrid interaction · Unpaved roads

List of Symbols

a	Geogrid aperture dimension (mm)
a_{eq}	Equivalent geogrid aperture dimension ($=(a_M \cdot a_{CM})^{1/2}$) (mm)
a_{CM}	Geogrid aperture width along the cross machine direction (mm)
a_M	Geogrid aperture width along the machine direction (mm)
ASM	Geogrid aperture stability modulus (N m/°)
B	Diameter of the loading plate (mm)
D_n	Particle diameter for which n % in mass of the remaining particles are smaller than that diameter (mm)
D_i	Representative fill particle diameter (mm)
D_{max}	Maximum fill particle diameter (mm)
$f_{a/D}$	Reduction factor for the influence of the ratio a_{eq}/D_{max}
G_f	Fill material shear modulus (kPa)
G_s	Subgrade material shear modulus (kPa)
GPF	Geogrid property factor (dimensionless)
H	Fill thickness (m)
J	Reinforcement tensile stiffness (kN/m)
$J_{5\%}$	Reinforcement secant tensile stiffness at 5 % strain (kN/m)
N	Number of load repetitions during cyclic loading (dimensionless)
N_r	Number of load cycles for a given surface rut depth in the reinforced fill (dimensionless)

✉ Ennio M. Palmeira
palmeira@unb.br

Ivonne A. G. Góngora
ivonnnegg_86@yahoo.com

[1] Department of Civil and Environmental Engineering, Faculty of Technology, University of Brasília, Brasília, DF 70.910-900, Brazil

N_u	Number of load cycles for a given surface rut depth in the unreinforced fill (dimensionless)
p	Pressure on the fill surface (kPa)
TBR	Traffic benefit ratio ($=N_r/N_u$) (dimensionless)
TBR_{max}	Maximum value of TBR (dimensionless)
t_{GG}	Average geogrid thickness (m)
t_M	Average thickness of the grid members parallel to the machine direction (mm)
t_{CM}	Average thickness of the grid members parallel to the cross-machine direction (mm)
T_{max}	Reinforcement tensile strength (kN/m)
α_b	Fraction of grid members' lateral area available for bearing in the grid aperture (dimensionless)
α_s	Fraction of grid area which is solid in plan (dimensionless)
δ	Vertical settlement of the loading plate or rut depth (mm)
ϕ_f	Fill material friction angle (°)
ϕ_s	Subgrade friction angle (°)
γ_f	Fill material unit weight (kN/m^3)
γ_s	Subgrade unit weight (kN/m^3)
ε_{max}	Maximum reinforcement strain (%)
τ	Shear strength of the subgrade (kPa)
ξ	Correction factor for the influence of the reinforcement on soil properties (dimensionless)

Introduction

The use of geosynthetics can be very effective to reinforce gravel layers on compressible and weak subgrades, particularly in the case of unpaved roads. These roads represent typically over 70 % of the road network of a country such as Brazil and are extremely important for the economy of the country as they allow the transportation of products from agricultural, mining and forestry industries, for instance, as well as for security reasons. They are also present in construction sites and parking areas and can be very important for providing access for isolated communities to educational and health services.

When built over weak subgrades the traffic of heavy vehicles and climatic factors can accelerate the degradation of the road, requiring constant maintenance works to avoid or minimize traffic disruption and economic losses. Geosynthetics can be used in this type of work in different functions, such as drainage, filtration, protection, separation and reinforcement. Some types of geosynthetics can fulfill more than one function in an unpaved road or a railway track, like nonwoven geotextiles, which can provide drainage and separation between a good quality fill material and a fine grained subgrade. Although being capable of also functioning as reinforcement, geotextiles are less effective than geogrids as reinforcement because of their usually lower tensile stiffness (typically in the case of nonwoven geotextiles) or less interaction with the surrounding soils.

Over the past four decades several researchers have investigated the beneficial effects of geosynthetic reinforcement in low reinforced fills on weak subgrades in the field and in laboratory experiments with particular reference to unpaved roads [1–9]. Several design approaches for unreinforced and reinforced unpaved roads on weak subgrades are available in the literature, particularly for roads on soft and saturated fine grained soils ([10–15], for instance). Most of the current design methods are based on limit equilibrium analysis, some degree of empiricism and simplifying assumptions. As a consequence, the influence of the limitations inherent to such assumptions on the method accuracy cannot be avoided. The available methods may consider, in different degrees, the influence of relevant factors related to the problem, such as type and properties of the reinforcement, the effects of traffic, degradation of the materials under repeated loading and membrane effect, for instance. However, the execution of an unpaved road on a weak subgrade is generally far from being as controlled as assumed in design methods or as in the case of paved roads or railways. Less construction control usually leads to significant road deformations and forces in the reinforcement being mobilised already during construction, which will influence road performance and that are still not considered in current design methods [5].

Giroud and Han [15] developed a comprehensive design method for unreinforced and geosynthetic reinforced unpaved roads that takes into account the strength of the subgrade and of the fill material, the number of load repetitions (truck axle loads) and reinforcement type and mechanical properties for prescribed values of road surface rut depths at the end of the road life. The innovative aspect of the method was the introduction of the geogrid aperture stability modulus (ASM) [16] as the geogrid mechanical property to be considered in design. ASM has been proposed as an index test to measure in-plane stiffness of a geogrid based on a torsional load applied to a grid junction. As torsion of the grid junction will cause bending of the adjacent grid members, it is likely that ASM and the grid tensile stiffness (J) are related to some extent, particularly under elastic load conditions. However, most of the available grids are composed of slender longitudinal and transverse members and interaction between gravel particles and grid members in an unpaved road is likely to result in loading conditions far from elastic in the field. Simac et al. [17] criticized the adoption of ASM as the only performance property of a geogrid and suggested that the design method would be significantly more generic and applicable if calibrated to average tensile strengths at 2–5 % strain. Results reported by Sprague [18], Tang [19],

Tang et al. [20], Góngora and Palmeira [9] and Cuelho et al. [21] have shown very poor or no correlation between ASM and pavement rutting intensity. On the other hand, other numerical and experimental studies in the literature have indicated the relevance of the reinforcement tensile stiffness on the performance of reinforced unpaved roads and railway ballasts [22–28, for instance].

Geosynthetic reinforcement can also be used in reinforced low fills on loose sandy soils or on collapsible soil deposits. Different assumptions to those applied to saturated fine grain soil foundations must be assumed for those subgrades. The use of geocells or ground improvement techniques can be considered for such loose subgrades. However, in general these solutions can be significantly more expensive and time consuming than using a single reinforcement layer at the base of the road fill. Although bearing some similarities to the conventional case of roads on soft ground, to the knowledge of the authors design methods for geosynthetic reinforced low fills on loose subgrades have not been developed.

Interaction between soil and reinforcement is of utmost importance for the performance of low fills on compressible subgrades. Thus, this paper addresses soil–reinforcement interaction by presenting a study aimed at identifying relevant soil–reinforcement interaction properties with regard to the reinforcement of low fills on weak subgrades, with particular reference to unpaved roads. However, some results and conclusions obtained may be extended to other similar situations. The geogrid reinforcements were selected or assembled in the laboratory so that a sensitivity analysis could be made, with the influence of a specific parameter being enhanced or attenuated with respect to those of the others trying to quantify its relevance to the road performance. The test methodology, results and discussions are presented in the following items. Additional benefits brought by reinforcement such as improvement in fill performance after surface repair and less fill particle breakage are presented and discussed in a companion paper [29].

Experiments

Equipment

A large apparatus was used in the tests on reinforced and unreinforced fill layers on compressible subgrade. The equipment consisted of a rigid tank 1200 mm in diameter and 520 mm high, as shown in Fig. 1. The internal smooth walls of the tank were lubricated with double layers of plastic film and oil to minimize friction with soils. The fill was loaded at its surface by a 200 mm diameter steel plate. A cylinder connected to a hydraulic system provided the vertical cyclic load on the loading plate with a frequency of 1 Hz and a maximum vertical stress transferred to the road surface equal to 560 kPa. A load cell measured the vertical load applied on the plate and displacement transducers allowed for the measurement of platen vertical displacements and vertical displacements at points on the fill material surface (Fig. 1). Total pressure cells (55 mm diameter, 6 mm thick) were installed at two different depths in the subgrade layer, i.e., at 50 and 150 mm from the fill–subgrade interface, on the axis of the loading plate. The cells were calibrated buried in the same subgrade soil and with the same properties as those employed in the tests. A data logger Lynx ADS 2000 and a microcomputer were used to acquire and process the instrumentation readings. The tests were interrupted when the vertical displacement of the loading platen reached 75 mm.

Materials

The cross-section of the unpaved road consisted of a gravel fill 300 mm thick on a 220 mm thick loose sand subgrade. All tests were carried out under dried conditions. The authors acknowledge that mainly because of the low thickness of the subgrade, such geometrical conditions do not represent accurately some typical problems involving the use of low reinforced fills, such as in unpaved roads, because in the field the subgrade layer would be much thicker. However, the main objective of the research was to investigate the influence of soil–reinforcement interaction properties on the performance of low reinforced fills on compressible ground, for which unpaved roads can be considered as similar structures. In this context, a loose sand subgrade was chosen just as a compressible layer underneath the gravel capable of subjecting the latter layer to deformations similar to those found in situations, such as in unpaved roads or railway tracks on compressible ground. In addition, it allowed quicker and simpler test preparations, with comparisons between the performance of several reinforced and unreinforced systems under the same subgrade conditions. The results obtained should also be relevant for situations where low fills are indeed built on loose granular deposits, as commented in the previous section of this paper. A loose sandy subgrade was also employed in tests on reinforced and unreinforced roads carried out by Cancelli et al. [30]. Similar test arrangements regarding subgrade material thickness and boundary conditions were employed by Brown et al. [26] and Hussaini [27] in studies on the influence of geogrid reinforcement on the performance of railway ballasts. Therefore, to some extent different results than those obtained in the tests reported in this paper might be expected had the subgrade material been thicker, but the authors believe that the identification and correlation

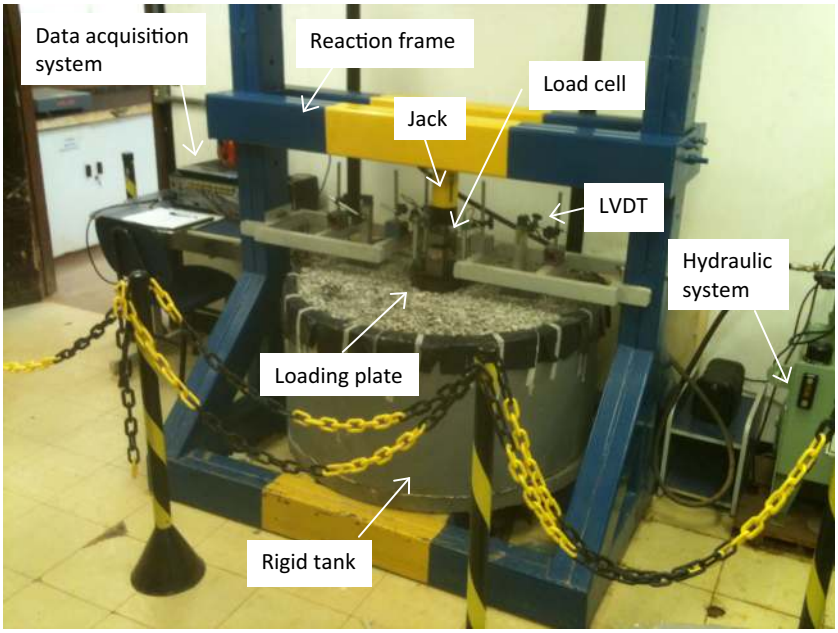

Fig. 1 View of the equipment during one of the tests

between relevant reinforcement properties and parameters influencing the performance of reinforced gravels on compressible ground will still be valid. In addition, different results, but probably similar conclusions, would be obtained if the subgrade consisted of a soft fine grained soil.

The main geotechnical properties of the soils used in the experiments are listed in Table 1. The fill consisted of gravel with 90 % of the mass of its particles with diameters varying between 1.5 and 21 mm, with average particle diameter (D_{50}) equal to 10.5 mm. The fill material was compacted in three layers (100 mm each) using static compaction to achieve a dense state, for which a friction angle of 43° was obtained in medium size (300 mm × 300 mm × 200 mm specimens) direct shear tests. The sand used in the subgrade had particle diameters varying between 0.2 and 2 mm (D_{50} of 1.4 mm). The subgrade layer was prepared using the sand rain technique with a height of fall of particles of 100 mm, in order to achieve a uniform and loose subgrade layer (relative density of 30 %). Under such conditions, a friction angle of 31° was obtained for the sand in direct shear tests. Despite being considered by many as an old fashioned testing technique, soil California bearing ratio (CBR) is still widely used in pavement related designs. For the sand used in the subgrade of the tests the value of CBR was equal to 1.6 %.

Table 1 Properties of the soils tested

Properties	Gravel	Sand
D_{85} (mm)[a]	16.0	1.63
D_{50} (mm)	10.51	1.01
D_{10} (mm)	1.49	0.46
Coefficient of uniformity (D_{60}/D_{10})	7.7	2.6
Specific gravity of soil solids	2.65	2.69
Unit weight (kN/m^3)	17.3	16.7
Relative density (%)	83	30
Friction angle (°)[b]	43	31
Cohesion (kPa)[b]	0	0
Los Angeles abrasion (%)	34	NA
California bearing ratio (%)	NA	1.6

NA not applicable or not available

[a] D_n particle diameter for which n % in mass of the remaining particles are smaller than that diameter

[b] Obtained from medium size (300 mm × 300 mm × 200 mm specimens) direct shear tests

Table 2 presents the main physical and mechanical properties of the reinforcements used in the test programme. Twelve geogrids and a woven geotextile were employed in the tests. Six geogrids (codes G1–6) and the geotextile (code GT) are commercially available products in the geosynthetic market, whereas the other geogrids (codes G7–12) were assembled in the laboratory with polypropylene strips. Although being presented by manufacturers as products with square apertures, the average aperture dimensions of geogrids G1–6 were measured before testing and the average values obtained are presented in Table 2. The dimensions of the apertures of these geogrids varied between 11 and 40 mm, with equivalent aperture dimensions (for rectangular apertures) varying between 12.9 and 32.3 mm. The equivalent aperture dimension is defined as the geometric mean of the sizes of

Table 2 Properties of the reinforcements and TBR values

Reinforcements	Polymer type	$J_{5\%}$ (kN/m)	T_{max} (kN/m)	ε_{max} (%)	ASM (N m/°)	t_M/t^b_{CM} (mm)	a_M/a^b_{CM} (mm)	a_{eq}	α_s	α_b	TBR
G1[a]	PET	893/300[b]	100/30[b]	8.0	0.033	1.8/1.2	18.4/21	19.7	0.37	0.80	121.0
G2	PET	811	80	13	0.074	2.0/1.0	23/35	28.4	0.32	0.83	78.7
G3	PP	417	18	10	0.040	1.2/0.6	15/11.6	13.2	0.37	0.83	6.5
G4[a]	PET	1165/300[b]	110/30[b]	12	0.036	1.9/1.4	18.5/14.1	16.2	0.35	0.81	72.6
G5	PP	474	38	10	0.107	1.6/1.0	26/40	32.2	0.31	0.83	2.9
G6	PP	474	43	8	0.029	1.3/0.8	11/15	12.8	0.35	0.81	4.0
G7	PP	72	15.0	14	0.043	0.4/0.4	30/30	30.0	0.65	0.59	1.3
G8	PP	117	15.0	14	0.067	0.6/0.6	30/30	30.0	0.65	0.59	1.3
G9	PP	164	15.0	14	0.095	1.0/1.0	60/60	60.0	0.45	0.74	2.1
G10	PP	300	15.0	14	0.103	1.2/1.2	60/60	60.0	0.45	0.74	2.3
G11	PP	416	21.0	12	0.133	1.0/1.0	30/30	30.0	0.56	0.67	1.7
G12	PP	261	11.5	12	0.054	1.0/1.0	60/60	60.0	0.36	0.80	1.4
GT[c]	PET	1022	103/50[b]	10	NA	0.5	NA	NA	1.00	NA	4.1

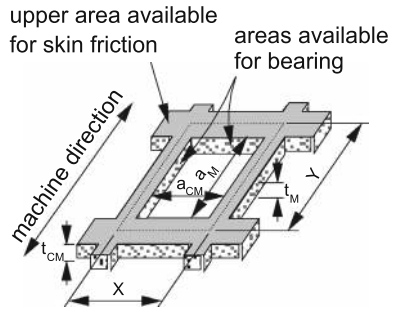

PET polyester, *PP* polypropylene, $J_{5\%}$ secant tensile stiffness at 5 % tensile strain, T_{max} tensile strength, ε_{max} maximum tensile strain, *ASM* aperture stability modulus (or torsional rigidity), t_M average thickness of the grid members parallel to the machine direction, t_{CM} average thickness of the grid members parallel to the cross-machine direction, a_M average aperture width along the machine direction, a_{CM} average aperture width along the cross-machine direction, a_{eq} equivalent aperture dimension $(=(a_M.a_{CM})^{1/2})$, α_s fraction of the grid area in plan which is solid, α_b fraction of the aperture area available for bearing, *TBR* traffic benefit ratio, *NA* not applicable

[a] Uniaxial grids

[b] Figure on the left is the property value along machine direction and on the right along cross-machine direction

[c] Woven geotextile

[d] All tensile properties obtained as per ASTM D6637 [31]

a rectangular aperture or the diameter of the largest circle inscribed in a triangular aperture [27]. Good correlation between reinforced ballast performance and the ratio between geogrid equivalent aperture dimension and ballast particle diameter was obtained by Hussaini [27].

The commercial geogrids tested were biaxial products with the exception of grids G1 and G4. The secant tensile stiffness at 5 % tensile strain ($J_{5\%}$, as per ASTM D6637 tensile test method) of geogrids G1–6 varied between 417 and 1135 kN/m and their fraction of solid area in plan (α_s = fraction of the total grid area available for friction—one side of the grid layer only, Table 2) varied between 0.32 and 0.37. The thickness of the grid members depended on the direction considered (machine or cross-machine directions) and average values varied between 0.6 and 2.0 mm. Values of ASM (as per ASTM WK24635 test method-standardization of this test method is in progress) for grids G1–6 varied between 0.029 and 0.107 N m/°. Table 2 also presents the fraction (α_b) of the lateral internal area of the grid aperture available for bearing, calculated as shown in the drawing in that table. The value of α_b varies little (between 0.8 and 0.83) for geogrids G1–6.

As mentioned above, biaxial grids G7–12 were assembled in the laboratory using polypropylene strips. The manufacture of these grids was intended to allow the variation of some specific grid properties while others would remain constant, or nearly constant, which would be very difficult to achieve with commercial grids. This procedure allowed a better evaluation of the influence of a specific grid property. Different conditions were adopted at the grid junctions (intersection between longitudinal and transverse grid members) in the assembling process of grids G7–12 (Table 2). In grids G7, G9, G11 and G12 each longitudinal and transverse member was fixed by a flat headed pin at the junction to favour rotation between these members. Grids G8 and G10 had the transverse and longitudinal members fixed with epoxy glue, which can be considered as a close approximation to the junction condition found in commercially available geogrids. All the other characteristics (raw material, spacing between members and member thickness and width) of grids G7 and G8 and of G9 and G10 were the same (Table 2), but the glue between transverse and longitudinal members influenced a little some of the properties. These different junction conditions were adopted to allow variation of grid ASM, keeping other geogrid physical and mechanical properties constant such as the ratio between fill particle size and grid aperture size, for instance. Values of $J_{5\%}$ (ASTM D6637 [31]) for the geogrids G7–12 were in the range 72–416 kN/m (Table 2). The ASM (ASTM WK24635 [32]) values for these grids varied between 0.043 and 0.133 N m/° and the value of α_s (between 0.36 and 0.65) in some cases was considerably greater than those of geogrids G1–6. The thickness of the grid members varied between 0.4 and 1.2 mm for geogrids G7–12 and their area available for bearing (α_b) varied between 0.59 and 0.8.

The woven geotextile tested was used for comparison purposes and consisted of a polyester product with a secant tensile stiffness at 5 % strain of 1022 kN/m. This value of stiffness is close to that of the stiffest geogrid tested (geogrid G4, $J_{5\%}$ = 1165 kN/m: machine direction). Additional information on the geotextile properties is presented in Table 2.

All reinforcements had their extremities folded in the fill material to improve anchorage conditions. No reinforcement anchorage failure was noticed during the experimental programme.

Results

Load–Displacement Behaviour

Figure 2a, b show results of vertical loading plate displacement versus number of load repetitions for reinforced and unreinforced fills. The unreinforced fill reached the maximum plate vertical displacement (75 mm) after a number (N_u) of load repetitions of 2810. The number of load repetitions for reinforced tests varied between 3755 and 340,068, depending on the reinforcement considered. In general, the commercial geogrids (G1–6) yielded larger values of N at maximum plate displacement (Fig. 2a) than the laboratory assembled geogrids (G7–12, Fig. 2b), particularly in the case of the fill reinforced with G1. Compared with the performance of most of the commercial geogrids, that of the geotextile was quite poor, with maximum plate displacement having been reached with a value of N equal to 11,437, but still well above the value obtained for the unreinforced fill. It should be pointed out that some unreinforced and reinforced tests were repeated to assess the repeatability of the testing methodology and the differences between test results were less than 6 %, which can be considered quite satisfactory.

The values of traffic benefit ratio (TBR) for the fills tested are presented in Fig. 3a, b and in Table 2. TBR is commonly used to evaluate the beneficial effects of reinforcement in paved and unpaved roads and is defined as the number of load repetitions in a reinforced fill divided by the number of load repetitions in the unreinforced fill for the same rut depth at fill surface. The TBR values obtained varied between 1.34 and 121, with smaller values being observed for the tests with geogrids G7–12. For the geotextile reinforced fill the value of TBR was equal to 4.1, which is greater than the values obtained in the tests with the laboratory assembled grids G7–12 (TBR between 1.3

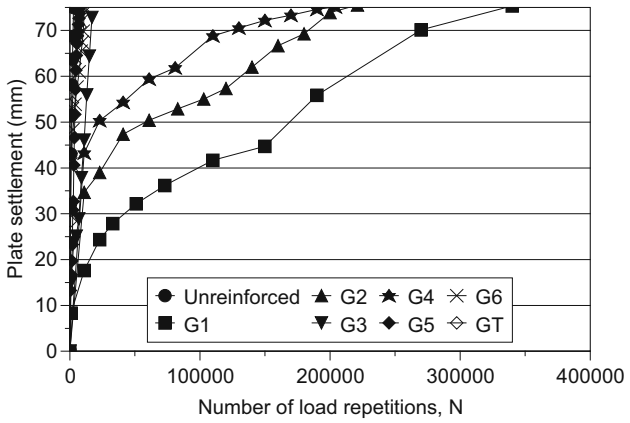

(a) Geogrids G1 to G6 and woven geotextile (GT).

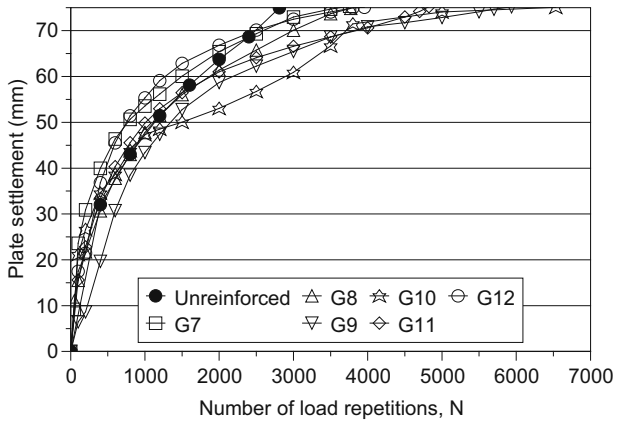

(b) Geogrids G7 to G12.

Fig. 2 Plate vertical displacement versus number of load repetitions

and 2.3) and in tests with grids G5 and G6 (TBR = 2.9 and 4.0, respectively). The largest TBR value (=121) was obtained for the fill reinforced with geogrid G1. This value is considerably larger than the usual values obtained in tests on unpaved roads on fine grained saturated soils (usually less than 15). The larger values obtained in the present work are due not only to the reinforcement presence but also because of the increase in shear strength due to compaction of the initially loose sand subgrade caused by the repetitive loading. In this sense, it would be expected that better interlock between geogrid and fill particles would enhance reinforcement performance and improve subgrade compaction conditions during cyclic loading. In addition, adherence between a geogrid and a granular subgrade is generally greater than with a saturated fine grained subgrade. Much larger values of TBR were obtained by Cancelli et al. [30] in tests on reinforced roads on a similar sandy subgrade. It should also be pointed out that even in tests with fine grained subgrade soils large values of TBR have been reported. For instance, Perkins et al. [33] report a reinforced test of a road on a subgrade with CBR equal to 1.5 % that was interrupted at a value of N_r of approximately 330,000 and a plate vertical displacement of 13 mm, because a stable and very low plate displacement to N_r ratio had been reached. Extrapolation of the test result to the target rut depth of 25 mm under such rate would yield a value of TBR of the order of 106. A TBR value above 100 for a rut depth of 25 mm would also have been obtained by Palmeira and Antunes [8] in a geogrid reinforced road on a subgrade with CBR of 8 % had the fill gravel particles not been broken after a value of N_r of 243,000. Results presented by Cancelli and Montanelli [34] show a TBR value of approximately 160 for a rut depth of 20 mm in tests on reinforced and unreinforced roads on a silty clay subgrade. Other examples of large values of TBR are reported by Perkins [35].

From the results in Table 2 it can be noted that geogrids with similar values of ASM (like grids G1, G3 and G4) yielded very different TBR values. The same happened in tests with geogrids with similar values of $J_{5\%}$ (like G5, G6 and G11), but to a lesser extent. This shows that reinforcement mechanical properties are not the only relevant parameters for reinforcement performance, as will be discussed later in this paper.

Figure 4a, b show vertical displacement profiles along the fill surface for the different systems tested for the value of N at the end of the unreinforced test. It can be noted that for distances from the loading plate centre greater than 1.3 plate diameters the vertical displacements were negligible. Geogrids G1–6 reduced fill surface displacements between 33 and 85 % with respect to the unreinforced test (Fig. 4a), depending on the geogrid considered. The presence of the woven geotextile reduced the vertical displacements by 23 %. The reductions obtained for the fills reinforced with geogrids G7–12 were smaller, ranging from 4 to 23 % (Fig. 4b).

Vertical Stresses in the Subgrade

The total vertical stresses at depths equal to 50 and 150 mm from the subgrade surface are depicted in Fig. 5 for a value of N equal to that at the end of the unreinforced test ($N = 2810$). As expected, larger vertical stresses occurred closer to the fill–subgrade interface and the stress intensity depended on the presence and type of reinforcement. Figure 5a shows that the presence of geogrids G1–6 caused a significant reduction in vertical stresses transferred to the subgrade, particularly closer to the fill–subgrade interface (depth of 50 mm). The best results were obtained for tests with the stiffest geogrids (G1, G2 and G4), although the results for G2 seem too low. It should be noted that the accuracy of pressure cell

measurements can be influenced by several factors, particularly in tests under cyclic loading. Displacement or rotation of the cell from its original position and changes in density of the surrounding soil during the test may affect its readings. Although factors such as these may explain some discrepancies among vertical stress values in Fig. 5a, the results suggest a consistent pattern of stress reduction in the subgrade as a function of geogrid tensile stiffness and geometry.

Figure 5b presents vertical stresses 50 and 150 mm deep in the subgrade for tests with geogrids G7–12 for N equal to the value obtained at the end of the unreinforced test. In this case the best result in terms of vertical stress reduction was obtained in the test with geogrid G10, which is the grid with the second highest tensile stiffness and the thickest one among geogrids G7–12. The results obtained for grids G8 and G12 were similar to those of the unreinforced test, which can be explained by the fact that G8 is very extensible and thin and G12, although stiffer than G8, is very open (large apertures).

Figure 6 shows the vertical stress at a depth from the subgrade surface equal to 50 mm in reinforced tests normalized by the vertical stress measured in the unreinforced test at the same depth for N equal to the value at the end of the unreinforced test. This figure shows clearly that the vertical stresses obtained in tests with the stiffest grids ($J_{5\%}$ between 811 and 1165 kN/m) were less than 37 % of the value obtained in the unreinforced test. For most of the laboratory assembled grids (G7–12) the vertical stresses were 66–100 % (between 57 and 87 kPa, Fig. 5) of that of the unreinforced test. It should be noted that differences among results are due not only to differences in tensile stiffness but also in aperture size, surface roughness and grid members shape and thickness.

The greatest reductions in vertical stress were obtained in tests with the stiffest geogrids (G1, G2 and G4) which were also the ones with ratios between grid aperture and fill particle sizes close to the optimum value, as will be seen later in this paper. The results obtained in the roads reinforced with geogrids G7–12 are also consistent in this regard. These grids have aperture–fill particle diameter ratios outside the most efficient range and low tensile stiffness (Table 2).

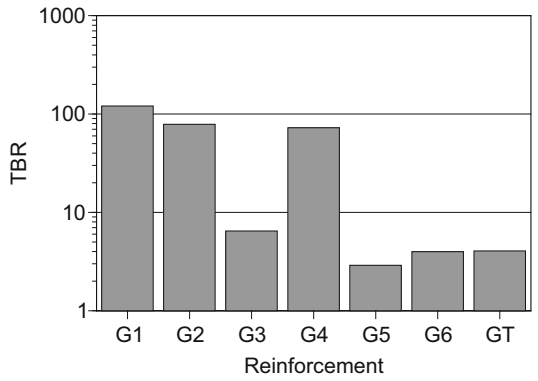

(a) Geogrids G1 to G6 and geotextile (GT).

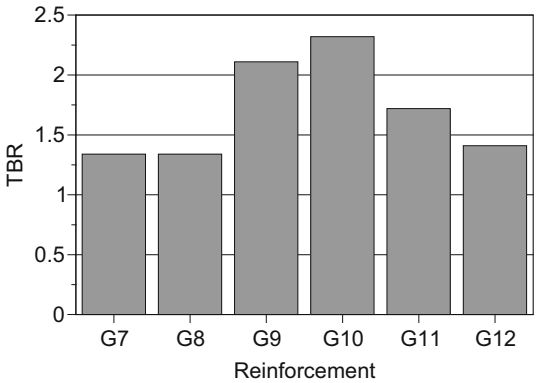

(b) Geogrids G7 to G12.

Fig. 3 Values of traffic benefit ratio (TBR)

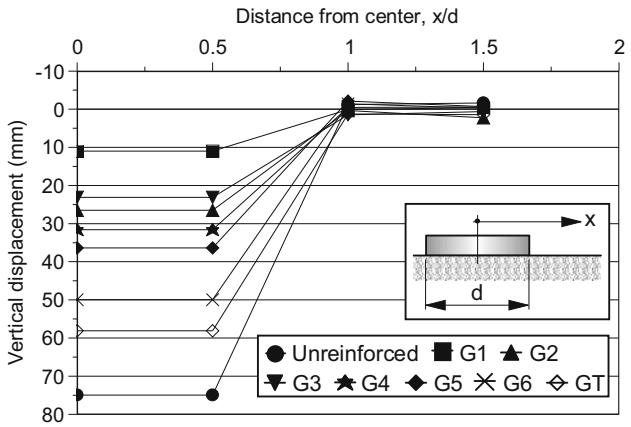

(a) Geogrids G1 to G6 and GT.

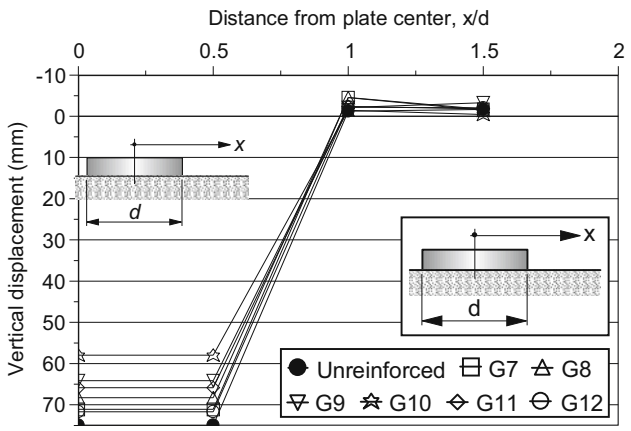

(b) Geogrids G7 to G12.

Fig. 4 Vertical displacement profiles along fill surface

Road Performance Versus Reinforcement Properties

Influence of Geogrid Geometrical Characteristics

Figure 7a presents the variation of TBR with the ratio between geogrid equivalent aperture dimension (a_{eq}) and fill average particle diameter (D_{50}). For comparison purposes this figure also shows results obtained from Cuelho et al. [21] (TBR vs. a_{eq}/D_{50}), Brown et al. [26] (ρ vs. a_{eq}/D_{50}, where ρ is the plate settlement for a number of load repetitions of 3000) and Hussaini [27] (LRSI vs. a_{eq}/D_{50}, where LRSI is the lateral spread reduction index, defined as the ratio of the difference in lateral displacement of unreinforced and reinforced ballast to the lateral displacement of unreinforced ballast). The results in Fig. 7a provide a measure of the efficiency of the reinforcement in improving road performance, but it should be noted that Brown et al. [26] and Hussaini [27] investigated the performance of reinforced and unreinforced railway ballasts and assessed reinforcement beneficial effects in terms of reductions in displacements. The results in Fig. 7a show that the most efficient a_{eq}/D_{50} ratio is approximately equal to 2 for the fill material used in the present work. A significant drop in the value of TBR takes place for a_{eq}/D_{50} values smaller than 1.5 or greater than 2.7. The data from Brown et al. [26] yielded to an optimum aperture size ratio of 1.8, which is close to the one obtained in the present work. The optimum aperture size obtained by Hussaini [27] was equal to 1.2, which is smaller than the previous values. For the broad graded fill material (coefficient of uniformity, CU = 123) used by Cuelho et al. [21] the most efficient a_{eq}/D_{50} ratio was considerably larger ($\cong$3.9). The results in Fig. 7a highlight the influence of the type of fill material on the optimum aperture size and suggest that for uniform or close to uniform fill materials the optimum a_{eq}/D_{50} ratio falls in the range 1.2–2.

A narrower range of variation of the optimum aperture–particle diameter ratio can be observed in Fig. 7b, where the results are plotted in terms of aperture equivalent dimension–fill material maximum particle diameter ratio (a_{eq}/D_{max}). In this case, the optimum a_{eq}/D_{max} value varied between 0.7 and 1.35 for fill materials with very different CU values, including the broad graded material used by Cuelho et al. [21]. The optimum a_{eq}/D_{max} for the grids tested in the present work was equal to 0.94, obtained for geogrid G1. Fernandes et al. [36] report very good performance of a geogrid reinforced railway sub-ballast for an a_{eq}/D_{max} ratio of 1.25. Numerical simulations of pull-out tests using the discrete element method (DEM) conducted by McDowell et al. [37] indicated that for low (less than 5 mm) pull-out displacements the highest pull-out forces were mobilized for a grid aperture–maximum ballast particle diameter ratio of 0.9, whereas for higher pull-out displacements (close to 30 mm) the optimum ratio was equal to 1.4. The values reported by Fernandes et al. [36] and those found in the DEM simulations are consistent with the range presented in Fig. 7b. Despite the narrower range of variation of the optimum ratio a_{eq}/D_{max} for the fill materials in Fig. 7b with respect to that of a_{eq}/D_{50}, the steep decline in TBR values (at different rates depending on the soil considered) for slight changes in that ratio cannot be neglected. Other factors certainly must influence to some extent the optimum a_{eq}/D_{max} (or a_{eq}/D_{50}) value, such as shape and surface characteristics of the fill particles, geogrid and fill particles interaction with the subgrade soil and mechanical properties of geogrid longitudinal and transverse members, for instance.

It should be noted that the results in Fig. 7a, b were obtained in tests on grids with different values of tensile stiffness, which may have also influenced the results obtained. However, from those figures and Table 2 it can be noted that even among grids with similar values of tensile stiffness (grids G1, G2 and G4) the best performance was achieved by geogrid G1, which despite being less stiff than G4 (a_{eq}/D_{max} = 0.77, TBR = 72.6) had a a_{eq}/D_{max} ratio (=0.94) closer to the optimum value and presented a greater TBR value (=121). Similar results for tests with the same geogrid or with geogrids with similar values of tensile stiffness were obtained by Brown et al. [26], Cuelho et al. [21] and McDowell et al. [37] in laboratory, field and numerical studies, respectively.

Figure 7a, b show that the particle size to aperture ratios of grids G7–12 (assembled in the laboratory with thin plastic strips) fell outside the most effective a_{eq}/D_{max} range. This explains to some extent the poor performance of those grids in comparison with some of the commercial grids tested.

Figure 8a, b depict the relation between TBR and different parameters related to the geogrid geometry. Figure 8a presents TBR versus the fraction of the geogrid which is solid in plan (α_s). This is the area (one geogrid side only) available for skin friction along the geogrid surface. Despite the significant scatter (likely to be due to the influence of other concurrent factors), the results in Fig. 8a show a trend of TBR reduction with the increase of α_s. For grids with smooth surfaces larger values of α_s may be detrimental because the area available for bearing decreases with the increase of α_s. Figure 8a suggests a threshold value of 0.4 for α_s beyond which greater reductions in the value of TBR were observed for the geogrids tested. It can be demonstrated that for a uniform grid with square apertures, constant thickness and transverse and longitudinal members with the same width the values of α_b and α_s are related by

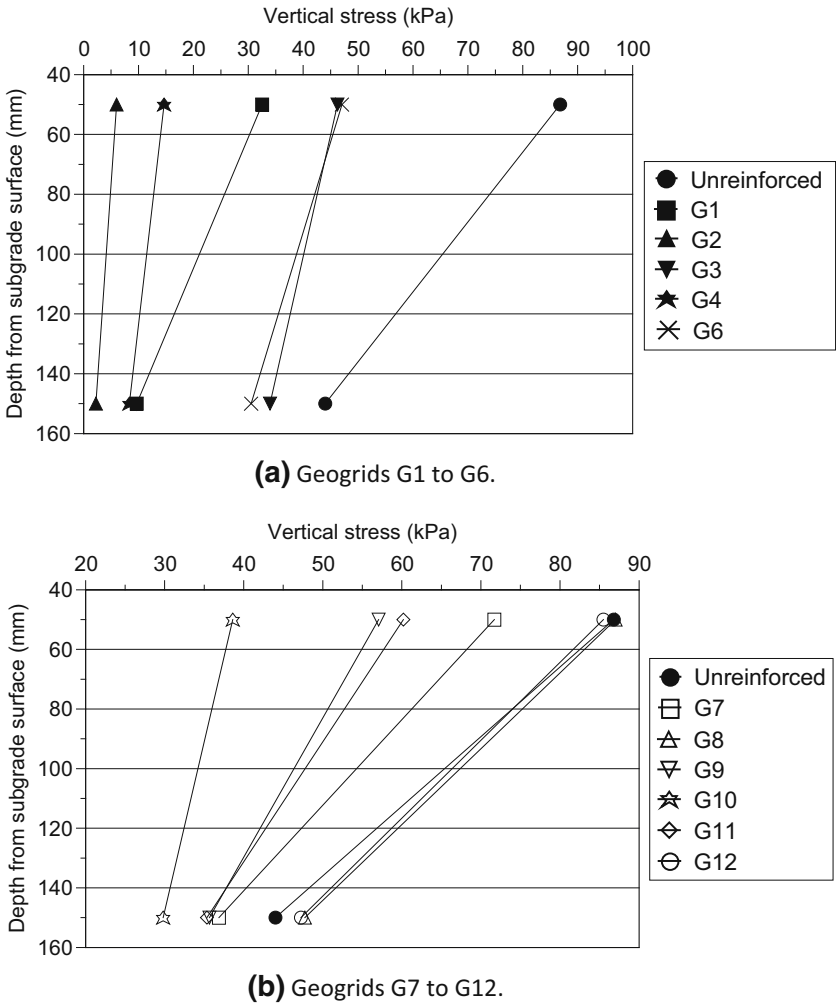

Fig. 5 Vertical stress in the subgrade

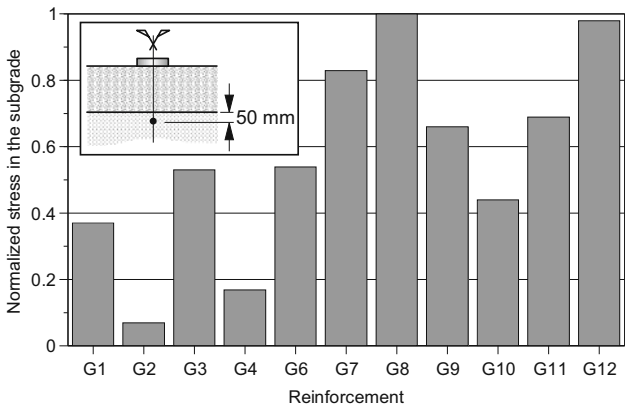

Fig. 6 Normalized vertical stress in the subgrade: $z = 50$ mm, $N = 2810$

$$\alpha_s = 1 - \alpha_b^2. \quad (1)$$

It should also be pointed out that for typical commercial grids the contribution of skin friction to granular soil–geogrid bond strength is significantly smaller than the contribution from the mobilized bearing forces along grid members [38–40].

The variation of TBR with the fraction of the grid aperture lateral area available for bearing (α_b) is shown in Fig. 8b, where a threshold value of α_b of the order of 0.75 can be noted beyond which greater increases in TBR were obtained. Contrary to what was observed for the fraction of the grid area in plan available for friction, the increase of available bearing area increased the value of TBR, particularly for values of α_b greater than 0.7.

Figure 9a, b show the relation between geogrid thickness and TBR in terms of average geogrid thickness (t_{GG}) normalized by the geogrid equivalent aperture dimension (a_{eq}) and average geogrid thickness normalized by the fill material average particle diameter (D_{50}), respectively. Again, despite the significant scatter the results show a trend of TBR increase with t_{GG}/D_{50} or t_{GG}/a_{eq}, with less scatter for the variation of TBR with t_{GG}/D_{50}. Geogrid thickness influences bearing capacity of grid members. The

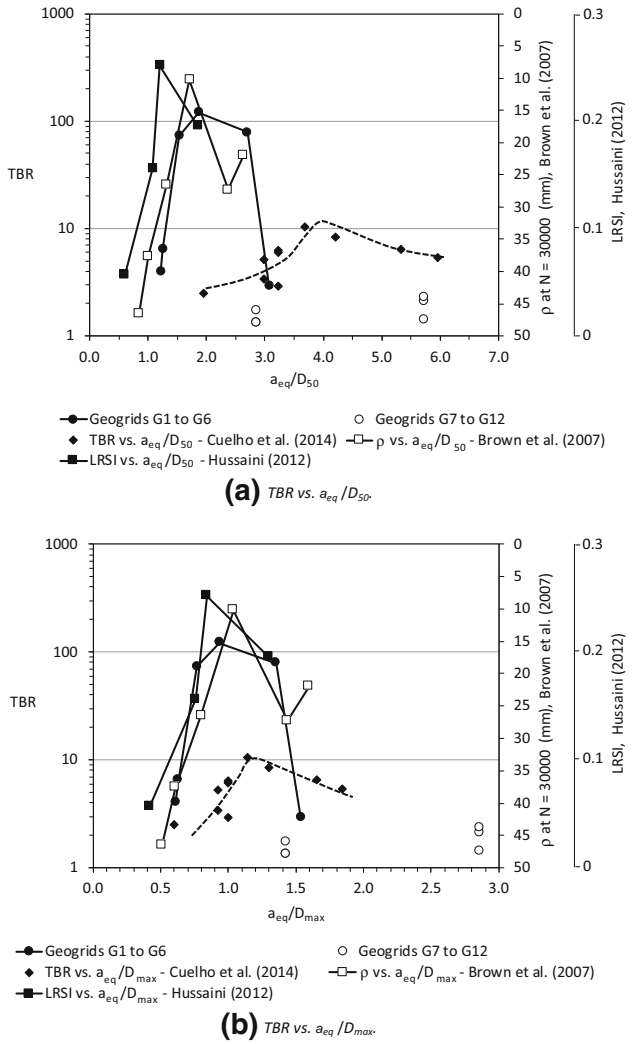

Fig. 7 TBR versus normalized grid aperture dimension

thicker the member and the greater the area available for bearing, the larger will be the bearing forces mobilized by grid members. The results in Figs. 7, 8 and 9 show the importance of grid geometrical characteristics and how they relate to fill material particle size with regard to the performance of low geogrid reinforced fills.

Discussion on Possible Correlations Between Geogrid Properties and Fill Performance

Figure 10a presents TBR versus ASM (geogrid ASM or torsional rigidity). No correlation can be noted between TBR and ASM for the geogrids tested, suggesting that the latter was not a relevant mechanical parameter regarding the performance of the reinforced fills tested. Table 2 and Fig. 2a show that the value of ASM for grid G1 (ASM = 0.033) was almost half the value for grid G2 (ASM = 0.076), but the performance of G1 was significantly better than that of G2. The value of ASM for geogrid G5 (ASM = 0.105) was significantly greater than those of G1 and G2, but the fill reinforced with G5 performed worse than those reinforced with G1 and G2. This lack of correlation between TBR and ASM is corroborated by the results obtained by Cuelho et al. [21], which are plotted in Fig. 10b. These authors performed real scale tests on experimental road sections on a fine grained subgrade (55 % passing the #200 sieve) using different types of commercially available geogrids with *ASM* and $J_{5\%}$ values ranging from 0.25 to 1.57 N m/° and 52 to 592 kN/m, respectively. The TBR values in Fig. 10b are those for a road surface depth of 62.6 mm (2.5 in.). No clear correlation can be seen between TBR and ASM in Fig. 10b either.

Figure 11a shows the variation of TBR with geogrid tensile stiffness ($J_{5\%}$). Despite some scatter, there is a clear trend of TBR increasing with $J_{5\%}$. The results also suggest that better fill performance was observed for values of $J_{5\%}$ greater than 400 kN/m. It is interesting to note that the best fill performance was achieved with geogrid G1, which is a uniaxial grid with values of tensile stiffness of 893 and 300 kN/m in each direction. The latter stiffness value is slightly smaller than 400 kN and the excellent performance of geogrid G1 is certainly due to a favourable combination of other properties, as will be quantified later in this paper. The same comments apply to the other uniaxial geogrid G4.

The results obtained by Cuelho et al. [21] are plotted in Fig. 11b where, despite the large scatter, an overall trend of TBR increase with the increase of geogrid tensile stiffness can be identified. It should be noted that the study reported by Cuelho et al. [21] was carried out under field conditions. So, a larger scatter would be expected in comparison with results obtained in the laboratory, where several factors that may influence test results can be better controlled.

From the results presented in Figs. 7, 8, 9, 10 and 11 one can conclude that the performance of a geogrid reinforcement depends on its physical and mechanical properties. The reinforcement tensile stiffness seems to be one of the key factors influencing the performance of the reinforced fill, but unfavourable combinations of other factors (t_{GG}/D_{50}, a_{eq}/D_{50} or a_{eq}/D_{max} ratios, for instance) may reduce the influence of the reinforcement stiffness. On the other hand, a rather low value of tensile stiffness can be compensated to some extent by appropriate combinations of other geogrid parameters. This can be better visualized in Fig. 12, where the values of TBR and of several physical and mechanical properties of the geogrids tested were plotted with geogrids with increasing values of TBR on the horizontal axis. In this figure it is clear that larger values of TBR were obtained for favourable combinations of geogrid properties. Greatest values of TBR are associated with

large values of t_{GG}/D_{50} and α_b, lower values of α_s and a_{eq}/D_{max} in or closer to the range 0.7–1.35. For instance, this is the case for geogrids G1, G2 and G4. Note that the reduction of TBR for G3 is a consequence of reductions in $J_{5\%}$ and t_{GG}/D_{50} and a_{eq}/D_{max} outside the optimum range. Similar comments apply to the other geogrids tested.

TBR Versus Some Geogrid Mechanical and Geometrical Properties

From dimensional analysis, the number (N_u) of load cycles on a low unreinforced fill on compressible subgrade for a given plate settlement (δ) to be reached can be expressed as:

$$N_u \approx f\left(\frac{\delta}{B}, \frac{H}{B}, \frac{\tau}{\gamma_f B}, \frac{\tau}{p}, \frac{G_f}{G_s}, \frac{G_s}{\tau}, \frac{\gamma_f}{\gamma_s}, \phi_f, \phi_s\right), \quad (2)$$

where N_u is the number of load cycles in the unreinforced case, δ is the vertical settlement of the surface load (rut depth), B is the diameter of the loaded area, H is the thickness of the fill, τ is a measure of the shear strength of the subgrade (undrained strength in soft saturated ground, for instance), γ_f is the fill material unit weight, p is the pressure on the fill surface, G_f is the fill shear modulus, G_s is the subgrade shear modulus, γ_s is the subgrade unit weight and ϕ_f and ϕ_s are fill and subgrade friction angles, respectively. It should be pointed out that some of the parameters in Eq. 2 may be irrelevant depending on the conditions under which δ is reached (elastic vs. plastic state, undrained vs. drained condition, etc.) or may vary during road deformation.

For a reinforced fill, the number of load repetitions to reach a surface settlement δ can be expressed as

$$N_r \approx f\left(\frac{\delta}{B}, \frac{H}{B}, \frac{\tau}{\gamma_f B}, \frac{\tau}{p}, \frac{G_f}{G_s}, \frac{G_s}{\tau}, \frac{\gamma_f}{\gamma_s}, \phi_f, \phi_s, \frac{J}{pB}, \frac{a}{D_i}, \alpha_b, \alpha_s, \frac{t_{GG}}{D_{50}}\right), \quad (3)$$

where N_r is the number of load repetitions in the reinforced case, J is the reinforcement tensile stiffness, a is the grid aperture dimension, D_i is a representative fill particle

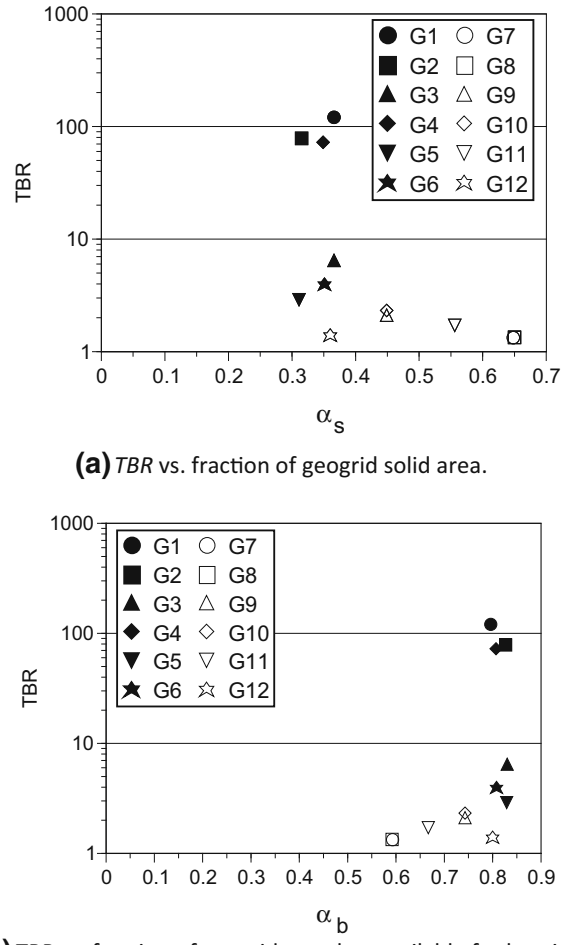

Fig. 8 Relations between fractions of geogrid solid and bearing areas and TBR

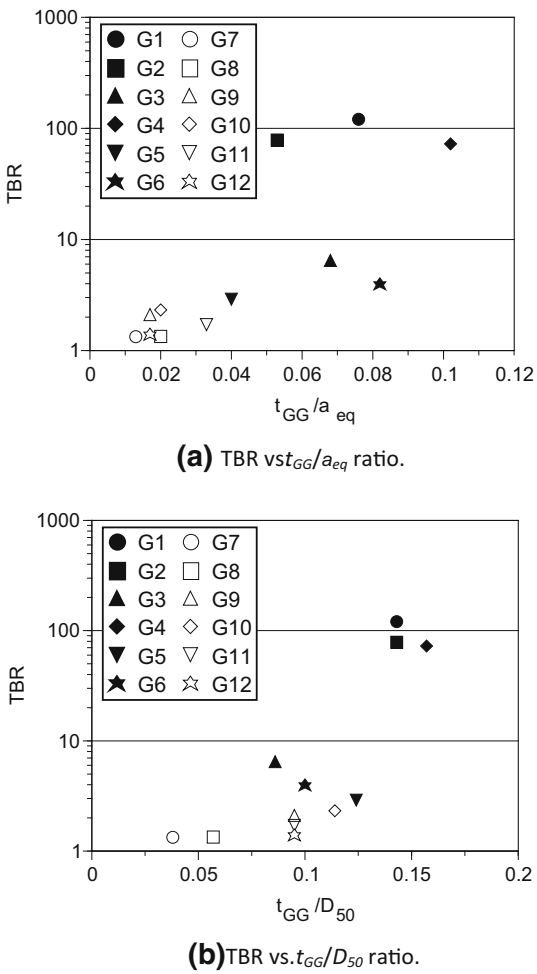

Fig. 9 Relation between geogrid thickness and TBR

diameter, α_b is the fraction of grid members' lateral area available for bearing in the grid aperture, α_s is the fraction of the total grid area which is solid in plan, t_{GG} is the geogrid average thickness and D_{50} is the average fill particle diameter.

Besides the parameters that would influence the number of load repetitions in the unreinforced road, Eq. 3 includes mechanical and physical properties of the geogrid, whose influences on fill performance have been discussed in previous sections of this paper. It should be noted that not only the value of α_b influences the magnitude of the passive resistance of the grid transverse members, but also the thickness (t_{GG}) of these members, because a grid can have a value of α_b equal or close to one but thin members (case of geogrids G7–12, for instance), which would yield to lower bearing strength and less efficiency in restraining the lateral deformation of the fill layer. Thus, the term t_{GG}/D_{50} is intended to take into account the influence of the geogrid thickness in Eq. 3. The ratio t_{GG}/a_{eq} could be equally employed for that matter; it was observed to yield similar results. However, the ratio t_{GG}/D_{50} was preferred because of less scatter in the correlation with TBR (Fig. 9b) and due to the fact that the influence of a had already been considered to some extent in the value of the ratio a/D_i. Grid member bending stiffness is also likely to influence the performance of the grid as a reinforcement to some extent [26, 41], but this influence has not been addressed in Eq. 3 because of the similar characteristics of flexibility of grid members for the geogrids tested, besides the difficulties in determining accurately the bending stiffness of the members of such geogrids.

The presence and type of reinforcement may influence differently some parameters in Eqs. 2 and 3. For instance, the reinforcement may reduce breakage of the fill gravel particles [8, 29, 36], which will delay the development of fill surface rutting in comparison with the unreinforced fill. Also, smaller vertical stresses are transferred to the subgrade for reinforced fills and hence different stress states will occur in reinforced and in unreinforced fill layers. Therefore, some stress dependent parameters in those equations (like shear modulus and friction angles) may have different values in Eqs. 2 and 3. As TBR is the ratio between N_r and N_u, assuming that a correction factor (ξ) will take into account the influences of the reinforcement

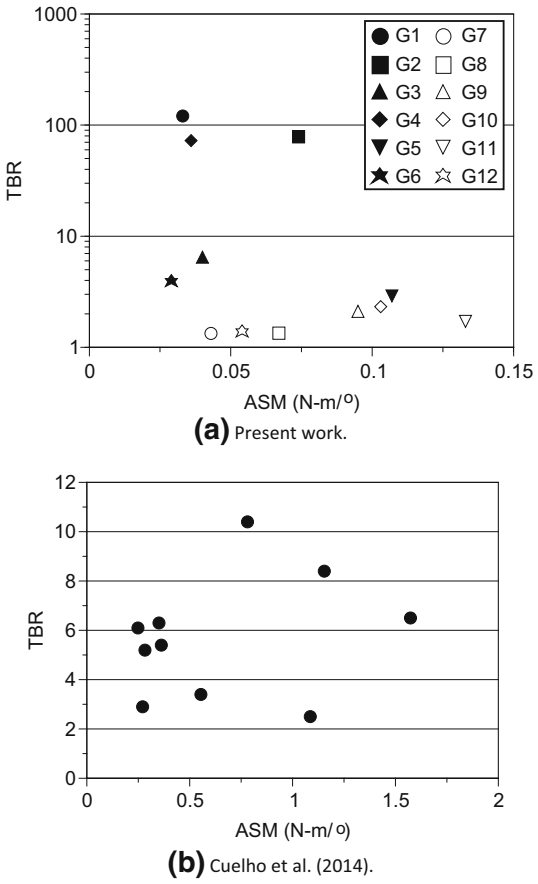

Fig. 10 Relation between TBR and geogrid aperture stability modulus (ASM)

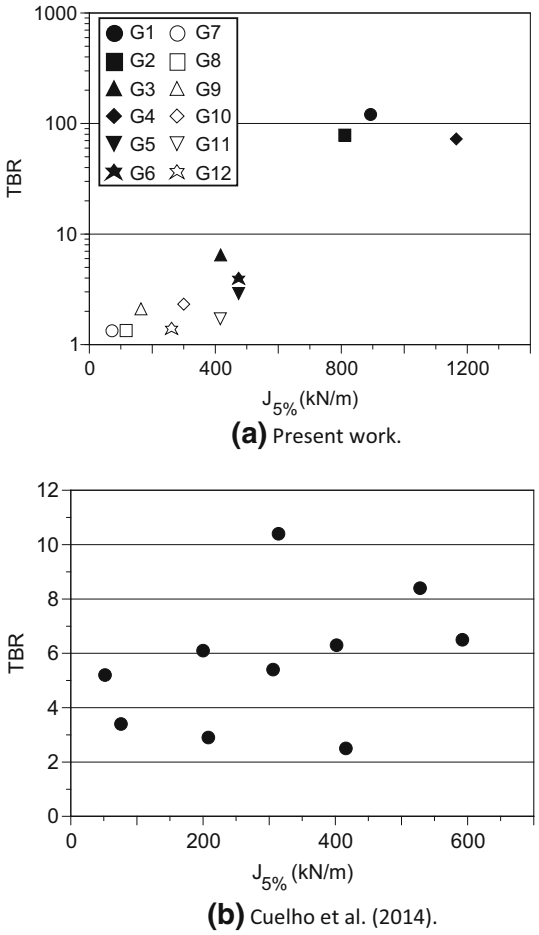

Fig. 11 Relation between TBR and geogrid tensile stiffness

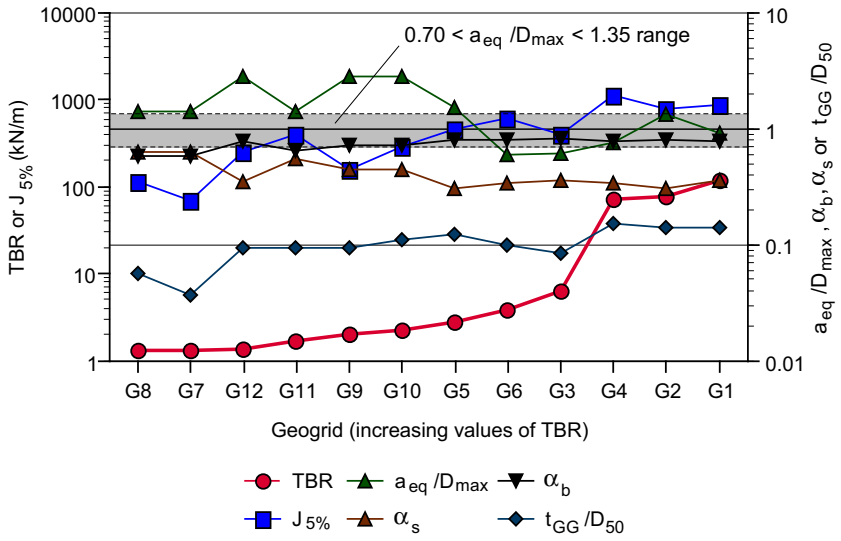

Fig. 12 Influence of different geogrid properties

on soil properties as discussed above (actually a different value of ξ should multiply each soil parameter in Eq. 3) one may expect that

$$\mathrm{TBR} \approx f\left(\frac{J}{pB}, \frac{a}{D_i}, \alpha_b, \alpha_s, \frac{t_{GG}}{D_{50}}, \xi\right). \quad (4)$$

Taking D_i equal to the maximum fill particle diameter (D_{max}, uniform fill materials) and the equivalent geogrid aperture value (a_{eq}), Eq. 4 can be rewritten as

$$\mathrm{TBR} \approx f\left(\frac{J}{pB}, \frac{a_{eq}}{D_{max}}, \alpha_b, \frac{t_{GG}}{D_{50}}, \xi\right). \quad (5)$$

The value of α_s was omitted in Eq. 5 because for a geogrid with square apertures and constant thickness and member width, the values of α_b and α_s are related to each other (Eq. 1). Some of the grids tested in this work do not have exactly square apertures, uniform thickness or member width. However, for the purposes of this analysis the comparisons between results from Eq. 1 and values of α_b and α_s for the grids tested yielded reasonably good agreement, as depicted in Fig. 13.

Figure 7a, b showed that the performance of the fill in terms of TBR can be influenced by the ratio a_{eq}/D_{max}. Taking the maximum fill particle diameter ($D_{max} = 21$ mm) as a reference, for the conditions of the tests performed in this work there was a significant reduction in TBR values for a_{eq}/D_{max} <0.6 or >1.5 (Fig. 7b). The most effective a_{eq}/D_{max} values are in the range 0.7–1.35, with optimum value of 0.94 (for grid G1). From Fig. 7b and Table 2 it can be seen that grids G5 to G12 have values of a_{eq}/D_{max} close to the limits of that range or well outside it (some of those grids with similar values of $J_{5\%}$, Fig. 12; Table 2) and they were the grids that presented smaller TBR values, although not necessarily negligible (TBR varying between 1.3 and 3.9).

As shown in Fig. 7, there is a nonlinear relation between TBR and the geogrid aperture dimension–fill particle diameter ratio. In this preliminary analysis, a simple way to take into account the influence of a_{eq}/D_{max} on the geogrid performance in the present work is to define a correction factor to be applied to TBR as a function of the value of a_{eq}/D_{max} given by

$$f_{a/D} = \frac{\mathrm{TBR}\left(\frac{a_{eq}}{D_{max}}\right)}{\mathrm{TBR}_{max}}, \quad (6)$$

where $f_{a/D}$ is the correction factor for a given value of a_{eq}/D_{max}, TBR is the traffic benefit ratio for a_{eq}/D_{max} and TBR_{max} is the maximum value of TBR obtained in the test for the optimum a_{eq}/D_{max} value. In Eq. 6 $f_{a/D}$ is maximum (=1) for a_{eq}/D_{max} equal to 0.94 (optimum value).

Curve fitting methods using known mathematical solutions were investigated to fit the results in Fig. 7 in order to obtain a more sophisticated equation for the correction

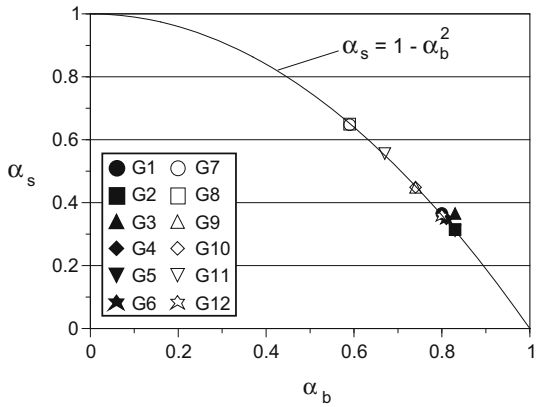

Fig. 13 Relation between α_s and α_b for the geogrids tested

factor presented in Eq. 6. Computing codes available for this type of analysis can provide sinusoidal or polynomial equations, for instance, with r^2 values greater than 0.89, but with limitations or inconsistencies for predictions for the entire range of a_{eq}/D_{max} tested in the current study. For the results in the range $0.6 \leq a_{eq}/D_{max} \leq 1.5$ (range for the commercial geogrids tested) equations (truncated Fourier series, for instance) relating TBR to a_{eq}/D_{max} can be obtained with values of r^2 as high as 0.999, but with significant deviations for predictions outside that range. Therefore, a simple relation as the one shown in Eq. 6 was preferred for the purposes of this study. Further investigation is in progress to refine this type of analysis.

Thus, for a correlation between TBR and different geogrids properties a geogrid property factor (GPF) is proposed and defined as

$$\mathrm{GPF} = \frac{J_{5\%}}{pB} \cdot \alpha_b \cdot \frac{t_{GG}}{D_{50}} \cdot f_{a/D} \cdot \xi. \quad (7)$$

Figure 14 shows the relation between TBR and GPF for the geogrids tested in the present work for a value of ξ equal to 1 (assuming no influence of the reinforcement on surrounding soils properties), where a satisfactory correlation can be observed. A greater rate of increase of TBR can be noted for values of GPF greater than 5×10^{-3}. It should be pointed out that Fig. 14 shows a consistent dependency of the reinforced fill performance on some physical and mechanical properties of the geogrid. Some statistical methods can be employed to assess the correlation between TBR and GPF. For instance, as an exercise the following were obtained:
Linear model:

$$\mathrm{TBR} = 2.17 + 117.2\mathrm{GPF} \quad \text{with} \quad r^2 = 0.958. \quad (8)$$

Hoerl nonlinear model:

$$\mathrm{TBR} = 73.418 \cdot 1.639^{\mathrm{GPF}} \cdot \mathrm{GPF}^{0.594} \quad \text{with} \quad r^2 = 0.960. \quad (9)$$

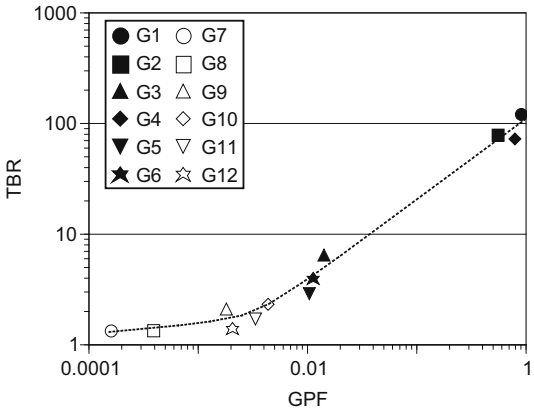

Fig. 14 Correlation between TBR and geogrid property factor

It should be stressed that the relationship in Eq. 7 was developed for the conditions of the present study (vertical displacement, fill and subgrade types, loading conditions, etc.). It may be applicable to other situations, but probably resulting in different TBR versus GPF curves than that in Fig. 14. The value of $f_{a/D}$ to be used will also depend on the properties and characteristics of the geogrid and fill material used.

Conclusions

This paper presented results of large scale tests on reinforced and unreinforced fills on a compressible subgrade aimed at studying the influence of some soil–reinforcement interaction parameters on the fill performance as a bearing layer. The main conclusions obtained in this study are presented as follows.

Different levels of improvement in fill performance were obtained depending on the reinforcement type and properties. Although the woven geotextile tested resulted in lower values of TBR than those obtained for some geogrids, it still provided significant improvement in fill performance. Except for the case of two of the geogrids assembled in the laboratory, the presence of the geogrid caused significant reductions in the vertical stresses transmitted to the subgrade.

The performance of a given geogrid reinforcement was markedly influenced by a combination of its mechanical and physical properties. The results obtained showed that geogrid tensile stiffness is a very important property with respect to reinforced fill performance. No correlation was observed between reinforcement ASM and fill performance for the conditions of the tests carried out. The ratio between aperture size and fill particle diameter was another important factor to reinforcement performance. It was also noted that the area available for bearing in the grid aperture and grid thickness were important physical parameters. On the other hand, an increase in the fraction of the grid total area available for friction in plan may be detrimental to its performance, particularly for smooth grids. This may not be the case for very rough geogrids and for geogrids incorporating out-of-plane anchoring elements, which were beyond the scope of this study.

The results obtained show that a geogrid reinforcement for a low fill layer (unpaved road or railway track, for instance) should be specified not only based on its tensile stiffness and strength but also considering the influence of other properties. The interaction between the geogrid and the surrounding soils plays a very important role in the reinforcement performance, and the results obtained showed the relevance of factors such as geogrid thickness

and aperture–fill particle diameter ratio. Regarding the latter, the geogrid should be chosen with that ratio equal or close to the optimum value. This is commonly neglected when specifying geogrid reinforcement. For the tests performed in this study the optimum value of the ratio between geogrid equivalent aperture dimension and maximum fill particle diameter was equal to 0.94 and the optimum value of that ratio considering the average fill particle diameter was equal to 1.8. It should be noted that the range of values of aperture–maximum (or average) fill particle diameter ratio within which large values of TBR were obtained was very narrow. Based on results obtained by other researchers it was also observed that the value of the optimum aperture–particle diameter ratio for broadly graded materials may vary significantly, depending on the CU of the fill material.

A satisfactory correlation between TBR and a geogrid property index defined as the product between various geogrid mechanical and physical properties was obtained for the geogrids and test conditions used in the present study. Although not simulating exactly an unpaved road or a railway track, the authors believe that the results obtained in the present study are relevant in such works. However, further research is required to improve the knowledge of soil–reinforcement interaction on the performance of low fills on compressible subgrades.

Acknowledgments The authors are indebted to the following institutions that contributed to the Research Programme described in this paper in different ways: The University of Brasilia, CNPq-National Council for Scientific and Technological Development, Capes/Brazilian Ministry of Education and the geogrid manufacturers.

References

1. Palmeira EM (1981) Geotextiles as reinforcement of embankments on soft soils. MSc Thesis, Federal University of Rio de Janeiro (in Portuguese)
2. Ramalho-Ortigao JA, Palmeira EM (1982) Geotextile performance at an access road on soft ground near Rio de Janeiro. In: Proceedings of the 2nd international conference on geotextiles, vol 1. IFAI, St. Paul, pp 353–358
3. Love JT, Burd HJ, Milligan GWE, Houlsby GT (1987) Analytical and model studies of reinforcement of a granular layer on a soft clay subgrade. Can Geotech J 24:611–622
4. Fannin RJ, Sigurdsson O (1996) Field observations on stabilization of unpaved roads with geosynthetics. J Geotech Eng ASCE 122(7):544–553
5. Palmeira EM (1998) Geosynthetic reinforced unpaved roads on very soft soils: construction and maintenance effects. In: Proceedings of the 6th international conference on geosynthetics, vol 2. IGS/IFAI, Atlanta, pp 885–890
6. Hufenus R, Rueegger R, Banjac R, Mayor P, Springman SM, Brönnimann R (2006) Full-scale field tests on geosynthetic reinforced unpaved roads on soft subgrade. Geotext Geomembr 24(1):21–37
7. Subaida EA, Chandrakaran S, Sankar N (2009) Laboratory performance of unpaved roads reinforced with woven coir geotextiles. Geotext Geomembr 27(3):204–210
8. Palmeira EM, Antunes LGS (2010) Large scale tests on geosynthetic reinforced unpaved roads subjected to surface maintenance. Geotext Geomembr 28:547–558
9. Góngora IAG, Palmeira EM (2012) Influence of fill and geogrid characteristics on the performance of unpaved roads on weak subgrades. Geosynth Int 19(2):191–199
10. Jessberger HL (1977) Load-bearing behaviour of a gravel subbase–non-woven fabric–soft subgrade system. In: Proceedings of the international conference on the use of fabrics in geotechnics, Paris, vol 1, pp 9–13
11. Bourdeau PL (1989) Modeling membrane action in a two-layer reinforced soil system. Comput Geotech 7:19–36
12. Steward J, Williamson R, Mahoney J (1977) Guidelines for use of fabrics in construction and maintenance of low-volume roads. Report PB-276 972. Forest Service, USDA, Portland
13. Giroud JP, Noiray L (1981) Geotextile-reinforced unpaved road design. J Geotech Eng ASCE 107(9):1233–1254
14. Houlsby GT, Jewell RA (1990) Design of reinforced unpaved roads for small rut depths. In: Proceedings of the 4th international conference on geosynthetics, The Hague, The Netherlands, vol 1, pp 171–176
15. Giroud JP, Han J (2004) Design method for geogrid-reinforced unpaved roads. I: development of design method. J Geotech Geoenviron Eng ASCE 130(8):775–786
16. Kinney TC, Xiaolin Y (1995) Geogrid aperture rigidity by in-plane rotation. In: Proceedings of Geosynthetics'95, Nashville, Tennessee, USA, vol 2, pp 525–537
17. Simac MR, Elton DJ, Gale SM (2006) Discussion of "Design method for geogrid-reinforced unpaved roads. I: Development of design method", by J. P. Giroud and Jie Han. J Geotech Geoenviron Eng ASCE 132:547–549
18. Sprague J (2001) In-plane rotational stiffness (A.K.A. torsional rigidity). TRI/Environ Lab Updates 1(1). www.geosynthetica.net/resources/inplane-rotational-stiffness-aka-torsional-rigidity/. Accessed 23 Feb 2015
19. Tang X (2011) A study of permanent deformation behaviour of geogrid reinforced flexible pavements using small scale accelerated pavement testing. PhD Thesis, Pennsylvania State University, Pennsylvania
20. Tang X, Chehab GR, Palomino A (2008) Evaluation of geogrids for stabilising weak pavement subgrade. Int J Pavement Eng 9(6):413–429
21. Cuelho E, Perkins S, Morris Z (2014) Relative operational performance of geosynthetic used as subgrade stabilization. Final Project Report, FHWA/MT-14-002/7712-251. Research Programs, State of Montana Department of Transportation, Montana
22. Brocklehurst CJ (1993) Finite element studies of reinforced and unreinforced two-layer soil systems. DPhil Thesis, University of Oxford
23. Burd HJ, Brocklehurst CJ (1994) Finite element studies of the mechanics of reinforced unpaved roads. In: Proceedings of the 4th international conferences on geosynthetics, The Hague, The Netherlands, vol 1, pp 217–221
24. Perkins SW, Ismeik M (1997) A synthesis and evaluation of geosynthetic-reinforced base layers in flexible pavements: Part I. Geosynth Int 4(6):549–604
25. Leng J, Gabr MA (2005) Numerical analysis of stress-deformation response in reinforced unpaved road sections. Geosynth Int 12(2):111–119
26. Brown SF, Kwan J, Thom NH (2007) Identifying the key parameters that influence geogrid reinforcement of railway ballast. Geotext Geomembr 25(6):326–335

27. Hussaini SKK (2012) An experimental study on the deformation behaviour of geosynthetic reinforced ballast. PhD Thesis, University of Wollongong, Australia
28. Góngora IAMG (2015) Geosynthetic reinforced unpaved roads: influence of physical and mechanical properties of the reinforcement. PhD Thesis, Graduate Programme of Geotechnics, University of Brasilia, Brazil (in Portuguese)
29. Góngora IAMG, Palmeira EM (2016) Assessing the influence of soil–reinforcement interaction parameters on the performance of a low fill on compressible subgrade—Part II: influence of surface maintenance. Int J Geosynth Ground Eng. doi:10.1007/s40891-015-0042-2
30. Cancelli A, Montanelli F, Rimoldi P, Zhao A (1996) Full scale laboratory testing on geosynthetics reinforced paved roads. In: Proceedings of the international symposium on earth reinforcement—IS Kyushu'96, Fukuoka, Kyushu, Japan, vol 1, pp 573–578
31. ASTM D6637 Standard test method for determining tensile properties of geogrids by the single or multi-rib tensile method. American Society for Testing and Materials, ASTM, West Conshohocken
32. ASTM WK24635. Determining the aperture stability modulus of geogrids (standardization of *ASM* test method in progress by ASTM). American Society for Testing and Materials, ASTM, West Conshohocken
33. Perkins SW, Ismeik M, Fogelsong ML (1999) Influence of geosynthetic placement position on the performance of reinforced flexible pavement systems. In: Proceedings of Geosynthetics'99, Boston, USA, vol 1, pp 253–264
34. Cancelli A, Montanelli F (1999) In-ground tests for geosynthetic reinforced flexible paved roads. In: Proceedings of Geosynthetics'99, Boston, Massachusetts, USA, vol 2, pp 863–878
35. Perkins SW (2001) Mechanistic-empirical modeling and design model development of geosynthetic reinforced flexible pavements: final report. Report no. FHWA/MT-01-002/991601A. State of Montana Department of Transportation/Federal Highway Administration, USA
36. Fernandes G, Palmeira EM, Gomes RC (2008) Performance of geosynthetic-reinforced alternative sub-ballast material in a railway track. Geosynth Int 15(5):311–321
37. McDowell GR, Harireche O, Konietzky H, Brown SF, Thom NH (2006) Discrete element modelling of geogrid-reinforced aggregates. Proc Inst Civ Eng Geotech Eng 159(GEI):35–48
38. Milligan GWE, Earl RF Bush DI (1990) Observations of photoelastic pull-out tests on geotextiles and geogrids. In: Proceedings of the 4th international conference on geosynthetics, The Hague, The Netherlands, vol 2, pp 747–751
39. Palmeira EM (2004) Bearing force mobilization in pull-out tests on geogrids. Geotext Geomembr 22(6):481–509
40. Calvarano LS, Cardile G, Gioffrè D, Moraci N (2013) Experimental and theoretical study on interference phenomena between the bearing members of different geogrids in pullout loading condition. In: Proceedings of Geosynthetics 2013, Long Beach, CA, USA, vol 1
41. Palmeira EM (2009) Soil–geosynthetic interaction: modelling and analysis. Geotext Geomembr 27(5):368–390